Available online at www.sciencedirect.com
ScienceDirect
Tetrahedron 63 (2007) 3850–3863
Tetrahedron

Sparsely substituted chlorins as core constructs in chlorophyll analogue chemistry. Part 3: Spectral and structural properties

Masahiko Taniguchi, Marcin Ptaszek, Brian E. McDowell, Paul D. Boyle and Jonathan S. Lindsey*

Department of Chemistry, North Carolina State University, Raleigh, NC 27695-8204, USA

Received 24 November 2006; revised 7 February 2007; accepted 9 February 2007
Available online 15 February 2007

Abstract—The availability of stable chlorins bearing few or no substituents has enabled a variety of fundamental studies. The studies described herein report absorption spectra of diverse chlorins, comparative NMR features of chlorins bearing 0–3 *meso*-aryl substituents, and X-ray structures of the fully unsubstituted chlorin and the oxochlorin.

1. Introduction

The preceding papers describe the synthesis and derivatization of stable chlorins bearing no *meso*-substituents, a single *meso*-substituent (5-, 10-, or 15-position), or two *meso*-substituents (10- and 15-positions).[1,2] The chlorins are stable owing to the presence of a geminal dimethyl group in the reduced, pyrroline ring. The availability of stable chlorins bearing few or no *meso*-substituents opens the door to a series of fundamental spectroscopic studies. Such studies may provide data that serve as benchmarks for understanding substituent effects in the naturally occurring chlorophylls (which bear a full complement of β-substituents) and support the design of complex molecular architectures containing synthetic chlorins.

In this paper, we describe the examination of a collection of sparsely substituted synthetic chlorins including the free base chlorin bearing no *meso*- or β-pyrrolic substituents (**H_2C**), its zinc chelate (**ZnC**), and analogues thereof. The studies include characterization of the ^{1}H NMR spectral properties of free base chlorins bearing 0–3 *meso*-substituents; full assignment of the ^{13}C NMR spectral properties of **H_2C** and **ZnC** accompanied by comparison with data for other model chlorins and for chlorophyll *a*; characterization of the absorption spectra of **H_2C**, metal chelates thereof [Mg(II), Cu(II), Zn(II), Pd(II)], and the diprotonated chlorin **H_4C^{2+}**; and determination of the X-ray structure of **ZnC** and the oxochlorin **Oxo-ZnC**. The results obtained from the synthetic chlorins begin to fill a lacuna that exists between the structurally complex chlorophylls and the simple synthetic chlorin model compounds prepared to date.

2. Results and discussion

The spectroscopic features of chlorins depend in part on the symmetry properties of the ligand. The π-chromophore of a chlorin has C_{2v} symmetry. The benchmark synthetic chlorins such as *meso*-tetraphenylchlorin (**H_2TPC**),[3] *syn*-octaethylchlorin (***syn*-H_2OEC**),[4] and chlorin (**H_2Chlorin**)[5,6] also have C_{2v} symmetry (Chart 1). However, the chlorin **H_2C** (and metal chelates thereof)[1,2] has C_s symmetry owing to the presence of the geminal dimethyl group. The location of the geminal dimethyl group at the 18-position and hydrogens at the 17-position results in the non-equivalence of the protons/carbons (e.g., H^{15} vs H^{20}, C^7 vs C^8) disposed on opposite sides of the vertical plane that bisects the N–N axis and the pyrroline ring. The lower symmetry of **H_2C** (and metal chelates thereof) is manifest in the NMR spectrum but not in the solution absorption or fluorescence spectrum.

The shorthand nomenclature for the chlorins described herein employs the following abbreviations with superscripts to denote substituents and their positions: P (phenyl), M (mesityl), and T (*p*-tolyl). The chlorins examined include those bearing no *meso*-substituents [(**H_2C**),[2] (**ZnC**)[1,7]]; one *meso*-substituent [(**H_2C-T^5**, **H_2C-M^{10}**, **H_2C-P^{10}**, **H_2C-P^{15}**, **H_2C-Br^{15}**),[2] (**ZnC-T^5**, **ZnC-P^{10}**),[1] (**ZnC-M^{10}**)[1,7]]; two *meso*-substituents (**H_2C-T^5M^{10}**, **ZnC-T^5M^{10}**);[8,9] and three *meso*-substituents (**H_2C-$T^5M^{10}P^{15}$**, **ZnC-$T^5M^{10}P^{15}$**).[10] Two oxochlorins [(**Oxo-H_2C**),[2] (**Oxo-H_2C-T^5M^{10}**)[11]] also were examined. The compounds are shown in Chart 2.

Keywords: Chlorin; NMR; Absorption spectra; X-ray.
* Corresponding author. Tel.: +1 919 5156406; fax: +1 919 5132830; e-mail: jlindsey@ncsu.edu

0040–4020/$ - see front matter © 2007 Elsevier Ltd. All rights reserved.
doi:10.1016/j.tet.2007.02.040

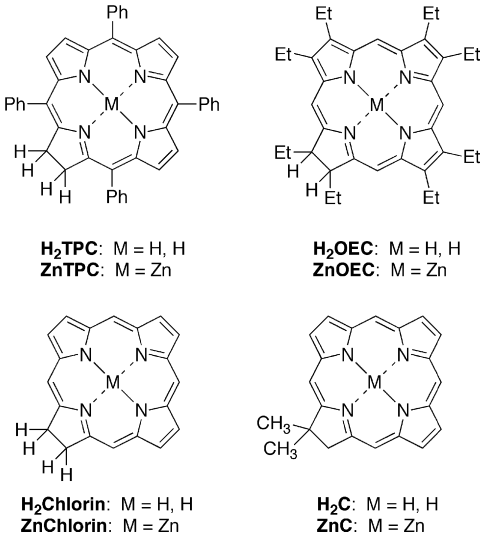

Chart 1.

2.1. ^{1}H NMR spectra of chlorins

Smith and co-workers studied ring current effects in chlorins versus porphyrins by comparing the NMR spectra of **H$_2$TPC** versus *meso*-tetraphenylporphyrin (**H$_2$TPP**) and **H$_2$OEC** versus 2,3,7,8,12,13,17,18-octaethylporphyrin (**H$_2$OEP**).[12] Although this fundamental study gave a full assignment of the *meso*-protons for **H$_2$OEC** and the β-protons for **H$_2$TPC**, the presence of substituents at the *meso*-positions (for **H$_2$TPC**) or β-positions (for **H$_2$OEC**) precluded a deeper understanding of the NMR properties of chlorins. The only example that we are aware of concerning assignment of the fully unsubstituted **H$_2$Chlorin** was reported in the early 1970s,[13] which left some uncertainty due to the experimental limitations at that time.

The chlorins examined herein by ^{1}H NMR spectroscopy were free base species rather than zinc chelates owing to the following reasons: (1) in general, the resonances of the protons attached to the chlorin macrocycles (**ZnC** through **ZnC-T^{5}M^{10}P^{15}**) tend to fall in a narrow range (with considerable overlap) for the zinc chelates but not the free base species. (2) The ^{1}H NMR spectrum of **ZnC** in $CDCl_3$ shows broadening of the resonances due to aggregation (which can be suppressed in THF-d_8). On the other hand, no aggregation was observed in $CDCl_3$ for free base chlorin **H$_2$C**.

The resonances of all *meso*- and β-protons of six chlorins with increasing number of aromatic substituents (from **H$_2$C** with no substituents to **H$_2$C-T^{5}M^{10}P^{15}** with three substituents) were assigned by HH COSY and NOESY spectra. A reversal of the chemical shift order of selected peaks was observed upon increasing the concentration to 100 mM for **H$_2$C-T^5**. Hence, all of the ^{1}H NMR spectra were recorded at identical concentration (20 mM) to avoid concentration effects on the chemical shifts of the resonances. ^{1}H NMR spectra are displayed in Figure 1 and chemical shifts are summarized in Table 1. See Chart 2 for the chlorin structures and numbering system.

Our assignments are based on the following observations: (1) coupling between β-protons in the same pyrrole ring (H^2–H^3, H^7–H^8, and H^{12}–H^{13}), (2) NOE between *meso*-protons and adjacent β-protons (H^5–H^3 and H^5–H^7; H^{10}–H^8 and H^{10}–H^{12}; H^{15}–H^{13} and H^{15}–H^{17}; H^{20}–H^2 and H^{20}–geminal dimethyl group at 18-position), and (3) NOE between *meso*-aryl protons and adjacent β-protons. Note that the introduction of three different aromatic rings with diverse resonances (~7.1 ppm for mesityl, ~7.5 and ~7.9 ppm for *p*-tolyl, ~7.6 and ~7.8 ppm for phenyl) enabled assignment for **H$_2$C-T^{5}M^{10}P^{15}**, which bears only one *meso*-proton (20-position).

The major findings are as follows.

(1) Chlorin **H$_2$C** versus porphine: all of the resonances of **H$_2$C** are shifted upfield compared to that of porphine (*meso*-position 10.37 ppm, β-position 9.53 ppm in $CDCl_3$)[17] due to the diminished ring current resulting from the saturation of the double bond at C^{17}–C^{18}. The order of the upfield shift ($\Delta\delta$) in **H$_2$C** compared to porphine is H^{15}, H^{20} (*meso*, ~1.3–1.4 ppm)≫H^2, H^{13} (β, ~0.6 ppm)>H^5, H^{10} (*meso*, ~0.5 ppm)>H^7, H^8 (β, 0.45 ppm)>H^3, H^{12} (β, ~0.3 ppm).

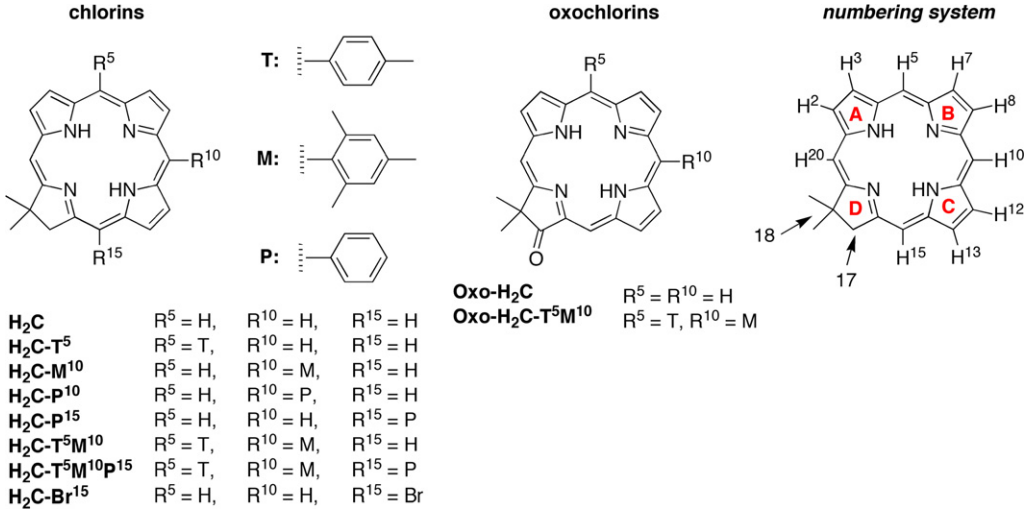

Chart 2.

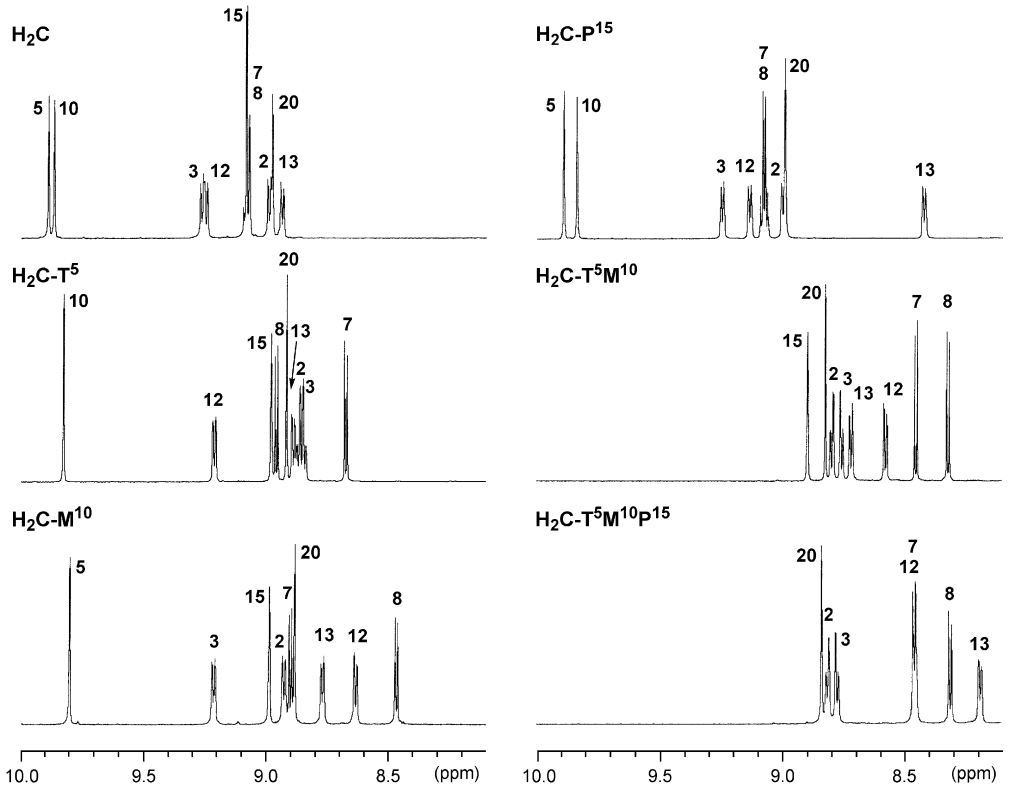

Figure 1. ^{1}H NMR spectra of chlorins with 0–3 *meso*-substituents (**H$_2$C**, **H$_2$C-T^5**, **H$_2$C-M^{10}**, **H$_2$C-P^{15}**, **H$_2$C-T^{5}M^{10}**, and **H$_2$C-T^{5}M^{10}P^{15}**) in $CDCl_3$ (20 mM) at 298 K.

In **H$_2$C**, the resonances of H^{15} or H^{20} are shifted upfield (~0.9–0.8 ppm) versus that of H^5 or H^{10}, which is comparable to the previous study of **H$_2$Chlorin** (0.7 ppm).[13] In addition, the resonance of H^{20} is slightly shifted upfield (0.1–0.07 ppm) compared to that of H^{15} due to the presence of the geminal dimethyl group at the 18-position.

(2) Effect of *meso*-aryl groups: (a) introduction of *meso*-aryl groups causes the β-positions adjacent to the aromatic ring (H^3 and H^7 for **H$_2$C-T^5**; H^8 and H^{12} for **H$_2$C-M^{10}** and **H$_2$C-P^{10}**; H^{13} for **H$_2$C-P^{15}**; H^3, H^7, H^8, and H^{12} for **H$_2$C-T^{5}M^{10}**; H^3, H^7, H^8, H^{12}, and H^{13} for **H$_2$C-T^{5}M^{10}P^{15}**) to shift upfield (~0.4–0.7 ppm) due to the ring current effect of the aryl ring. The degree of shielding was more pronounced with the mesityl versus the phenyl or *p*-tolyl group (~0.6 ppm vs ~0.4 ppm).

(b) The presence of a *meso*-aryl ring shields the entire adjacent pyrrole ring, as indicated by the chemical shift of the distal proton(s) of the adjacent pyrrole ring(s) [in **H$_2$C-T^5**, H^2 and H^8 are shifted upfield (~0.12 pm); in **H$_2$C-M^{10}**, H^7 and H^{13} are shifted upfield (~0.17 pm); in **H$_2$C-P^{15}**, H^{12} is shifted upfield (~0.11 pm)]. For chlorins that bear more than two *meso*-substituents, the shielding effect is additive. For example, H^{12} in **H$_2$C-T^{5}M^{10}P^{15}** shows the greatest upfield shift (0.78 ppm) owing to both the mesityl [$\Delta\delta$= 0.61 ppm for H^{12} in **H$_2$C-M^{10}**] and phenyl [$\Delta\delta$=0.11 ppm for H^{12} in **H$_2$C-P^{15}**] groups.

Table 1. ^{1}H NMR chemical shifts for free base chlorins with 0–3 *meso*-substituents[a]

Position		**H$_2$C** δ	**H$_2$C-T^5** δ ($\Delta\delta$)	**H$_2$C-M^{10}** δ ($\Delta\delta$)	**H$_2$C-P^{10}** δ ($\Delta\delta$)	**H$_2$C-P^{15}** δ ($\Delta\delta$)	**H$_2$C-T^{5}M^{10}** δ ($\Delta\delta$)	**H$_2$C-T^{5}M^{10}P^{15}** δ ($\Delta\delta$)	**H$_2$C-Br^{15}** δ ($\Delta\delta$)	**Oxo-H$_2$C** δ ($\Delta\delta$)
meso	5	9.89	—	9.81 (−0.08)	9.86 (−0.03)	9.89 (0)	—	—	9.81 (−0.08)	10.03 (+0.14)
	10	9.86	9.82 (−0.04)	—	—	9.84 (−0.02)	—	—	9.74 (−0.12)	10.11 (**+0.25**)
	15	9.08	8.98 (−0.10)	8.99 (−0.09)	9.03 (−0.05)	—	8.90 (−0.18)	—	—	9.98 (**+0.90**)
	20	8.98	8.91 (−0.07)	8.89 (−0.09)	8.91 (−0.07)	8.99 (+0.01)	8.83 (−0.15)	8.84 (−0.14)	8.89 (−0.09)	9.34 (**+0.36**)
β	2	8.99	8.87 (−0.12)	8.93 (−0.06)	8.95 (−0.04)	9.00 (+0.01)	8.80 (−0.19)	8.81 (−0.18)	8.95 (−0.04)	9.26 (**+0.27**)
	3	9.26	8.84 (**−0.42**)	9.21 (−0.05)	9.24 (−0.02)	9.24 (−0.02)	8.76 (**−0.50**)	8.77 (**−0.49**)	9.17 (−0.09)	9.41 (+0.15)
	7	9.08	8.67 (**−0.41**)	8.91 (−0.17)	8.97 (−0.11)	9.07 (−0.01)	8.45 (**−0.63**)	8.46 (**−0.62**)	9.02 (−0.06)	9.18 (+0.10)
	8	9.08	8.95 (−0.13)	8.47 (**−0.61**)	8.64 (**−0.44**)	9.07 (−0.01)	8.32 (**−0.76**)	8.31 (**−0.77**)	8.98 (−0.10)	9.23 (+0.15)
	12	9.24	9.21 (−0.03)	8.63 (**−0.61**)	8.82 (**−0.42**)	9.13 (−0.11)	8.58 (**−0.66**)	8.46 (**−0.78**)	9.19 (−0.05)	9.40 (+0.16)
	13	8.94	8.89 (−0.05)	8.77 (−0.17)	8.82 (−0.12)	8.42 (**−0.52**)	8.72 (−0.22)	8.19 (**−0.75**)	9.26 (**+0.32**)	9.31 (**+0.37**)
	17	4.66	4.61 (−0.05)	4.63 (−0.03)	4.64 (−0.02)	4.25 (**−0.41**)	4.59 (−0.07)	4.18 (**−0.48**)	4.67 (+0.01)	—
	18[b]	2.07	2.05 (−0.02)	2.06 (−0.01)	2.06 (−0.01)	1.99 (−0.08)	2.05 (−0.02)	1.97 (−0.10)	2.04 (−0.03)	2.12 (+0.07)

[a] In $CDCl_3$ (20 mM) at 298 K. Large chemical shifts from the reference chlorin are displayed in bold.
[b] Protons of the geminal dimethyl group (18-position).

(c) The introduction of the 15-phenyl group (**H_2C-P^{15}** or **H_2C-$T^5M^{10}P^{15}$**) shields the pyrroline ring: the resonances of the adjacent H^{17} (0.41 or 0.48 ppm) and geminal dimethyl group at the 18-position (~0.1 ppm) shift upfield.

(3) Effect of the bromo group: introduction of the 15-bromo group (**H_2C-Br^{15}**) causes the resonance of the adjacent pyrrole proton (H^{13}) to shift downfield ($\Delta\delta$=0.32 ppm), with no effect on the resonance of the adjacent pyrroline protons (H^{17}).

(4) Effect of the carbonyl group: introduction of the oxo group at the 17-position giving the oxochlorin (**Oxo-H_2C**) causes every resonance of the chlorin macrocycle to shift downfield. A significant downfield shift (0.9 ppm) is observed for the resonance of the adjacent proton (H^{15}), and large downfield shifts (~0.3 ppm) are observed for the resonances from the protons relatively close to the carbonyl group (H^{20}, H^{13}) as well as H^2 and H^{10}.

In summary, the resonances from the *meso*-protons are strongly shifted upfield by the structure change from porphyrin to chlorin, while those from the β-protons are shifted upfield by the presence of *meso*-aryl substituents. Knowledge of the spectroscopic properties of these simple chlorins has proved invaluable in clarifying the substitution pattern in more substituted chlorin macrocycles.[7]

2.2. ^{13}C NMR spectra of chlorins

The assignment of the ^{13}C NMR spectra of chlorins has been challenging due to three factors: (1) the complexity derived from the lower symmetry of the macrocycle versus porphyrins, (2) the presence of a large number of substituents, at least for naturally occurring chlorins, and (3) the large number of quaternary carbons. Recent advances in heteronuclear correlation 2D NMR techniques, such as HSQC (heteronuclear single quantum correlation) or HMBC (heteronuclear multiple-bond multiple quantum correlation), now make it possible to assign all carbon resonances, including those from quaternary carbons, of the chlorin macrocycle. Indeed, the complete assignment of methyl chlorophyllide has been carried out.[18] Although a handful of synthetic chlorins have been examined by ^{13}C NMR spectroscopy as benchmarks for chlorophyll,[19] full assignments of ^{13}C NMR spectra have so far been reported only for *meso*-tetrakis(*m*-hydroxyphenyl)chlorin (**H_2-*m*-THPC**),[15] **ZnOEC**,[16,20] and *meso*-tetramethylchlorinatonickel(II) (**NiTMC**).[21,22] The tetraarylchlorins are not ideal for fundamental studies of chlorin ^{13}C NMR spectra owing to the presence of four *meso*-substituents. By contrast, chlorophyll bears three unsubstituted *meso*-positions. On the other hand, the octaalkylchlorins bear a full complement of β-pyrrolic substituents. Again, the ^{13}C NMR spectrum of a benchmark chlorin lacking *meso*- and β-substituents has heretofore not been reported.

The resonances of all *meso*, α-, and β-carbons of a series of six synthetic chlorins were assigned on the basis of the results from gHSQC and gHMBC experiments. The representative gHMBC spectrum of **H_2C-T^5M^{10}** is shown in Figure 2.

Tertiary carbons [*meso*-(unsubstituted)- and β-carbons] were assigned in a straightforward manner by gHSQC experiments, aided by the assignment of all of the protons as discussed in the prior section. Quaternary carbons [*meso*-(substituted)- and α-carbons] were assigned by gHMBC experiments on the basis of the following observations:

(1) α-Pyrrole carbons were assigned on the basis of the cross signals between β-protons on adjacent carbons [e.g., C^{14}–H^{12} (^3J), C^{14}–H^{13} (^2J)]. In the case where adjacent *meso*-positions were unsubstituted, the cross signal between *meso*-protons [e.g., C^{14}–H^{15} (^2J)] was also used for assignments (Fig. 2, see cross signals 4a–4c).

(2) Quaternary *meso*-carbons: in gHMBC, cross signals between the *meso*-carbons and a chlorin macrocycle proton were not observed (a similar observation was reported by Hynninen and co-workers for bonellin dimethyl ester[23]). This makes the assignment of quaternary *meso*-carbons somewhat difficult. In the chlorins examined herein, the assignments of these quaternary *meso*-carbons were performed on the basis of the cross signal between *meso*-aromatic protons and the *meso*-carbon. For example, for a chlorin that bears a *p*-tolyl group at the 5-position (**H_2C-T^5**, **H_2C-T^5M^{10}**, or **H_2C-$T^5M^{10}P^{15}$**), the resonance of C^5 can be readily assigned by the cross signal between the *p*-tolyl protons adjacent to the chlorin macrocycle and C^5 (^3J). In the case where the 15-position bears a phenyl group (**H_2C-P^{15}** or **H_2C-$T^5M^{10}P^{15}$**), the resonance of C^{15} can be readily assigned by the cross signal between the phenyl protons adjacent to the chlorin macrocycle and C^{15} (^3J), together with the cross signal between H^{17} and C^{15} (^3J). For the case where the 10-position bears a mesityl group, C^{10} was not directly assigned because no cross signals were observed. In this case, C^{10} was assigned indirectly by elimination given the assignments of the other *meso*-carbons.

The α- and β-carbons were unambiguously assigned for **H_2C** and **ZnC** (when $\Delta\delta$ for pairs of resonances is <0.2 ppm) with the exception of carbons in the pyrroline ring (C^{16}, C^{17}, C^{18}, and C^{19}). The chemical shifts of a given pair of carbons at similar positions with respect to the pyrroline ring (but not equivalent owing to the presence of the geminal dimethyl group, e.g., C^2 and C^{13}, C^1 and C^{14}) are almost identical. When the chlorin bears *meso*-aryl substituent(s) (e.g., **H_2C-T^5M^{10}** and **H_2C-$T^5M^{10}P^{15}$**), the resonances were fully assigned including each quaternary carbon, because such substitution imparts chemical shifts to the otherwise nearly identical resonances of the carbons in the chlorin macrocycle.

The assigned chemical shifts of ^{13}C NMR spectra for porphine (**H_2P**), **H_2C**, **H_2-*m*-THPC**, **ZnP**, **ZnC**, and **ZnOEC** are summarized in Table 2 (in THF-d_8). The major findings are as follows.

(i) *meso*-Carbons: the resonances of **H_2C** or **ZnC** at C^{15} and C^{20}, which flank the pyrroline ring, are shifted upfield (~10 ppm) compared to that of the corresponding porphyrins **H_2P** or **ZnP**. On the other hand, the resonances of C^5 and C^{10}, which are distal to the pyrroline ring, do not show any significant changes.

(ii) β-Carbons: the resonances of all chlorins at the saturated site in the pyrroline ring (C^{17} and C^{18}) are shifted upfield

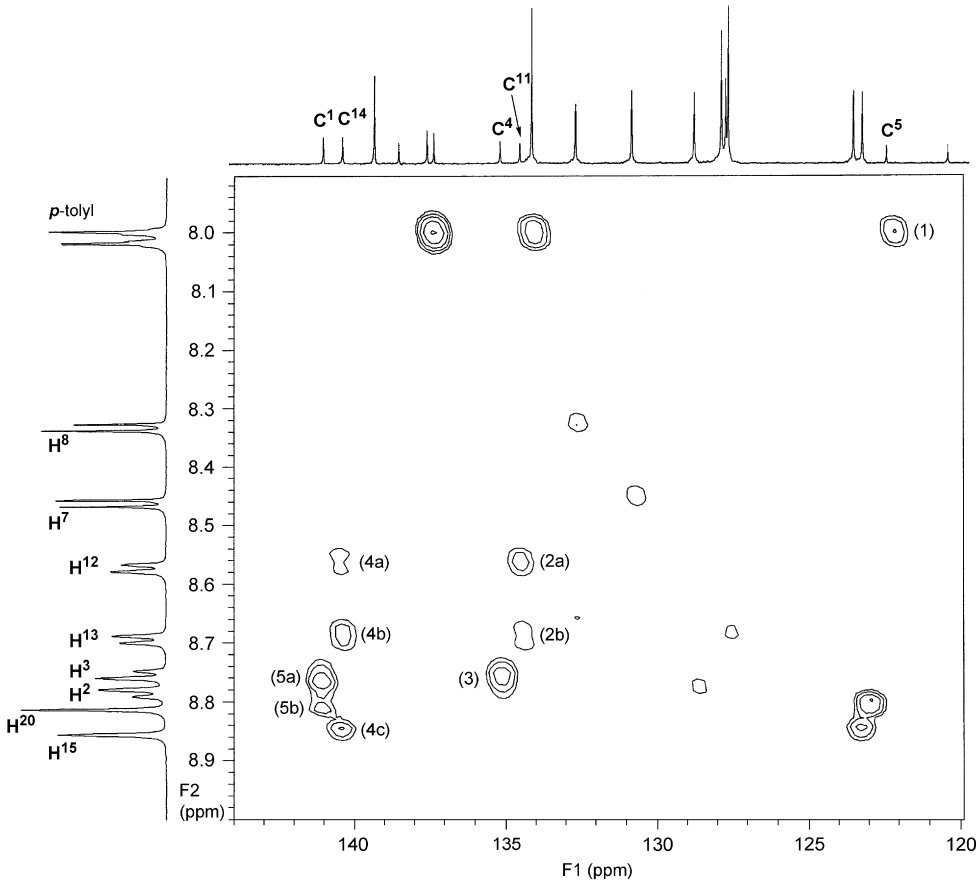

Figure 2. gHMBC spectrum of $\mathbf{H_2C\text{-}T^5M^{10}}$ (in $CDCl_3$, expanded). The following correlations were applied for the assignments: (1) *p*-tolyl protons–C^5 (^3J); (2a) H^{12}–C^{11} (^2J); (2b) H^{13}–C^{11} (^3J); (3) H^2–C^4 (^3J) and H^3–C^4 (^2J); (4a) H^{12}–C^{14} (^3J); (4b) H^{13}–C^{14} (^2J); (4c) H^{15}–C^{14} (^2J); (5a) H^2–C^1 (^2J) and H^3–C^1 (^3J); and (5b) H^{20}–C^1 (^2J). The correlations of cross signals are noted only for quaternary carbons. The other cross peaks are from the correlation of tertiary carbons, which were already assigned by gHSQC.

compared to that of the corresponding β-pyrrolic carbons in porphyrin **H_2P** or **ZnP**. The upfield shift is 80.8 and 86.2 ppm for **H_2C**, and 89.3 and 94.7 ppm for **ZnC**. In **H_2C**, the resonances of C^2 (C^{13}) and C^3 (C^{12}) are also shifted upfield, while C^7 (C^8) does not show significant changes, versus that of **H_2P**. In **ZnC**, the resonances of all the β-carbons are shifted upfield (7.7–13.1 ppm) versus that of **ZnP**.

(iii) α-Carbons: the resonances from the pyrroline ring (C^{16} and C^{19}) are shifted downfield (16.7 and 28.2 ppm for **H_2C**, 6.6 and 18.1 ppm for **ZnC**, respectively) compared to that of the porphyrin **H_2P** or **ZnP**.

(iv) Effects of *meso*-substituents in chlorin macrocycles: the resonances of the *meso*-carbons of ***m*-THPC** are shifted downfield (~15 ppm) compared to that of **H_2C**, due to the presence of *meso*-aryl substituents. To assess the effects of *meso*-substituents on the chemical shifts of carbons at sites other than the substituted carbon, the chemical shifts of α- and β-carbons for **H_2C** versus ***m*-THPC** (excluding the carbons adjacent to the pyrroline ring wherein the geminal dimethyl group gives a β-effect) were compared. The order of the chemical shifts of **H_2C** and ***m*-THPC** match each other (C^2, C^{13}<C^3, C^{12}<C^7, C^8<C^4, C^{11}<C^1, C^{14}<C^6, C^9). In addition, the respective chemical shift values are very similar in each case. These results indicate that, at least for the *meso*-phenyl groups compared herein, the *meso*-substituents typically alter the chemical shifts at the site to which they are attached, but have negligible effect on other carbons in the macrocycle (vide infra).

(v) Effects of β-substituents in chlorin macrocycles: the resonances of the β-carbons of **ZnOEC** are shifted downfield (~11 ppm) compared to that of **ZnC**. The respective chemical shift values of the α-carbons for **H_2C** and ***m*-THPC** are very similar, and the order of the chemical shifts of the α-carbons in **ZnC** and **ZnOEC** match each other (C^4, C^{11}~C^6, C^9<C^1, C^{14}). On the other hand, the resonances of the *meso*-carbons (C5 and C10) are shifted upfield by 7 ppm. Similar effects of β-alkyl substituents on the chemical shift of *meso*-carbons are observed for porphyrins: the resonance of the *meso*-carbon is shifted upfield ~9 ppm by the introduction of β-substituents (**H_2P** gives 106.0 ppm whereas **H_2OEP** gives 96.4 ppm,[24] **ZnP** gives 106.5 ppm whereas **ZnOEP** gives 97.4 ppm[24]). Understanding the effects of β-substituents would require the synthesis of a variety of β-substituted analogues of **ZnC**. In this regard, only a few analogues of **ZnC** bearing one or two β-substituents have been prepared to date.[7,25]

The ^{13}C NMR spectral resonances for five chlorins with increasing number of aromatic substituents (from **H_2C** with no substituents to $\mathbf{H_2C\text{-}T^5M^{10}P^{15}}$ with three substituents) and

Table 2. ^{13}C NMR chemical shifts for **H_2C** and **ZnC**

Position		**H_2P**[a] δ	**H_2C**[b] δ ($\Delta\delta$)[c]	***m*-THPC**[d] δ ($\Delta\delta$)[c]	**ZnP**[a] δ	**ZnC**[b] δ ($\Delta\delta$)[e]	**ZnOEC**[f] δ ($\Delta\delta$)[e]
meso	5	106.0	107.4 (+1.4)	122.0 (+16.0)	106.5	108.2 (+1.7)	100.9 (–5.6)
	10		107.0 (+1.0)			107.9 (+1.4)	
	15		97.2 (–8.8)	112.1 (+6.1)		95.7 (–10.8)	93.1 (–13.4)
	20		95.3 (–10.7)			93.5 (–13.0)	
β	2, 13	133.6	124.4 (–9.2)[g]	123.6 (–10.0)	140.0	126.9 (–13.1)[g]	137.8 (–2.2)
	3, 12		128.7 (–4.9)[g]	128.0 (–5.6)		132.3 (–7.7)[g]	143.0 (+3.0)
	7, 8		133.3 (–0.3)[g]	131.7 (–1.9)		128.0 (–12.0)[g]	139.5 (–0.5)
	17, 18		52.8 (–80.8)	35.4 (–98.2)		50.7 (–89.3)	54.3 (–85.7)
			47.4 (–86.2)			45.3 (–94.7)	
α	1, 14	147.2	141.0 (–6.2)[g]	139.8 (–7.4)	151.8	153.5 (+1.7)[g]	151.9 (+0.1)
	4, 11		135.9 (–11.3)[g]	134.1 (–13.1)		146.2 (–5.6)[g]	144.3 (–7.5)
	6, 9		153.0 (+5.8)[g]	151.5 (+4.3)		146.5 (–5.3)[g]	144.6 (–7.2)
	16		163.9 (+16.7)	167.6 (+20.4)		158.4 (+6.6)	163.9 (+12.1)
	19		175.4 (+28.2)			169.9 (+18.1)	

[a] Ref. 14 (in THF-d_8 at 298 K).
[b] In THF-d_8 at 298 K.
[c] $\Delta\delta$=δ of chlorin−δ of **H_2P**.
[d] Ref. 15 (in DMSO-d_6).
[e] $\Delta\delta$=δ of Zn chlorin−δ of **ZnP**.
[f] Ref. 16 (in THF-d_8).
[g] For clarity, the chemical shifts shown are the average of the two chemical shifts. Typically, the differences of the chemical shifts are less than 0.2 ppm.

oxochlorin (**Oxo-H_2C**) are summarized in Table 3. The spectra were obtained in $CDCl_3$. However, we note that the ^{13}C NMR spectrum of **H_2C** measured in either $CDCl_3$ or THF-d_8 showed neither a significant solvent effect on chemical shift (within 1.5 ppm) nor reversal of the chemical shift order. The introduction of a *meso*-aryl group causes a downfield shift of the *meso*-substituted carbon; the value of the $\Delta\delta$ is ∼16 ppm for the *p*-tolyl group and ∼14 ppm for the mesityl group. The effects of such *meso*-aryl substituents are insignificant on the chemical shifts of the α- and β-carbons ($\Delta\delta$<1.5 ppm). Introduction of the 17-oxo group (oxochlorin **Oxo-H_2C**) gives significant chemical shifts only at the reduced pyrrole ring: C^{16} and C^{19} are shifted upfield by 16.6 and 6.8 ppm, respectively.

The chemical shifts of **ZnC** and **H_2C** were compared to those of **13^2(*R*)-Chl *a***[26] and bonellin dimethyl ester[23] (Fig. 3). Bonellin dimethyl ester contains only one β-alkyl substituent in each of rings A and B. By contrast, **H_2C** has no such substituents, whereas **H_2OEC** contains a full complement of four β-alkyl substituents.

(a) **H_2C** versus bonellin dimethyl ester: the chemical shifts of **H_2C** and bonellin dimethyl ester are generally quite

Table 3. ^{13}C NMR chemical shifts for free base chlorins with 0–3 *meso*-substituents[a]

Position		**H_2C** δ ($\Delta\delta$)[b]	**H_2C-T^5** δ ($\Delta\delta$)[b]	**H_2C-M^{10}** δ ($\Delta\delta$)[b]	**H_2C-T^5M^{10}** δ ($\Delta\delta$)[b]	**H_2C-$T^5M^{10}P^{15}$** δ ($\Delta\delta$)[b]	**Oxo-H_2C** δ ($\Delta\delta$)[b]
meso	5	106.9	122.3 (+15.4)	107.2	122.5 (+15.6)	121.9 (+15.0)	105.8
	10	106.5	107.1	120.1 (+13.6)	120.4 (+13.9)	121.2 (+14.7)	107.7
	15	96.7	96.4	96.8	96.5	111.9 (+15.2)	96.3
	20	94.7	95.1	94.4	94.8	95.0	95.7
	2	123.7	*123.4*	*123.4*	123.3	123.8	126.6
	13	123.7	*123.6*	*123.9*	123.5	123.4	126.3
β	3	*128.1*	128.6	128.3	128.8	128.5	129.0
	12	*128.2*	128.6	127.4	127.7	127.2	127.9
	7	*132.6*	132.6	133.0	132.7	132.4	134.0
	8	*132.8*	132.4	131.3	130.8	131.2	134.9
	17	52.2	52.0	52.2	51.9	52.1	210.6 (+158.4)
	18	46.8	46.8	46.7	46.6	46.2	50.4 (+3.6)
	1	140.5	*140.4*	*139.8*	141.0	140.8	140.0
	14	139.8	*140.5*	*141.1*	140.4	141.0	137.6
α	4	134.7	135.4	*134.4*	135.2	135.8	137.0
	11	135.0	134.6	*134.9*	134.6	134.2	135.8
	6	151.6	152.8	*151.3*	152.4	153.1	*154.4*
	9	151.9	151.3	*152.8*	152.3	151.9	*153.1*
	16	163.3	163.9	163.0	163.5	162.8	146.7 (−16.6)
	19	174.9	174.5	175.3	174.9	174.7	168.1 (−6.8)

[a] In $CDCl_3$ at 298 K. The assignments within selected pairs of carbons (2,13; 3,12; 7,8; 1,14; 4,11; 6,9) given in italics could not be unambiguously distinguished and may be interchanged.
[b] $\Delta\delta$=δ of chlorin−δ of **H_2C** (given where the value is >3 ppm).

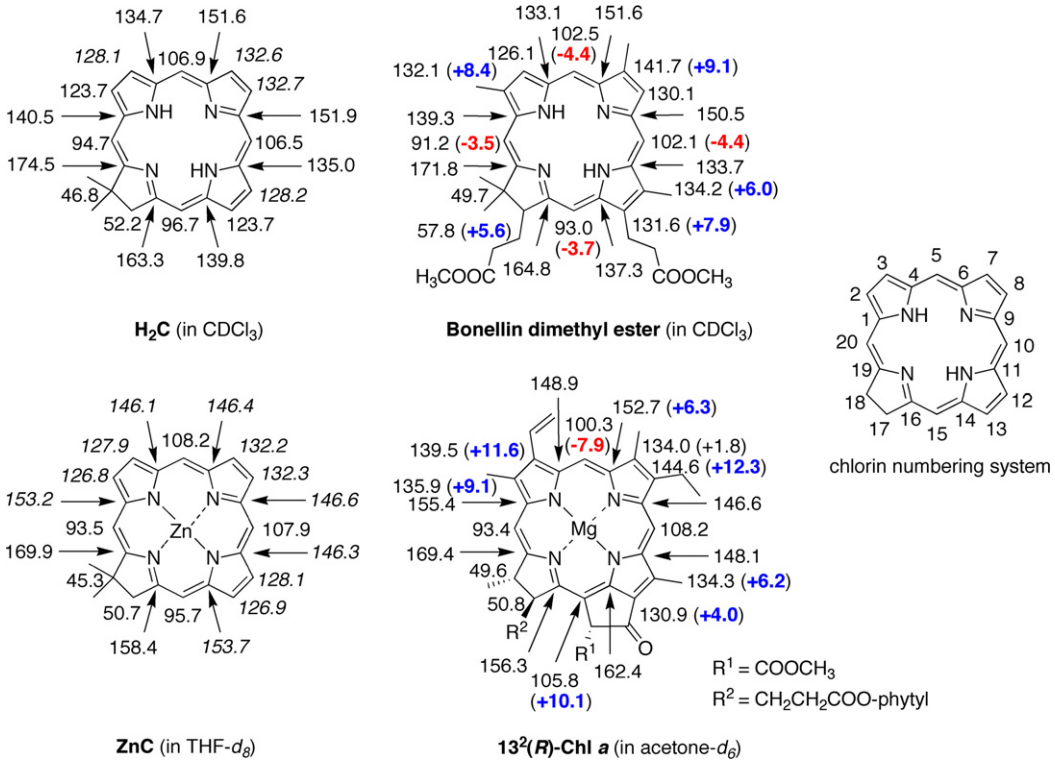

Figure 3. ^{13}C NMR assignments of **ZnC**, $\mathbf{H_2C}$, methyl chlorophyllide **13²(*R*)-Chl *a***, and bonellin dimethyl ester. The italicized numbers shown for $\mathbf{H_2C}$ or **ZnC** indicate resonances that were not unambiguously assigned (e.g., C^7 and C^8; C^3 and C^{12}) as described in Table 3. The parenthetic numbers denote $\Delta\delta$ of the resonance versus that in the corresponding free base chlorin $\mathbf{H_2C}$ or zinc chlorin **ZnC** (upfield shift given in red; downfield shift given in blue).

comparable. Bonellin dimethyl ester contains several pairs of adjacent quaternary carbons, for which assignments are made with difficulty using HMBC given that both carbons show the same cross peaks. By analogy with the simpler NMR spectrum of $\mathbf{H_2C}$, where no such pairs are present, we have tentatively revised the previous assignments[23] for two pairs of adjacent quaternary carbons (C^1 and C^2, and C^6 and C^7) in bonellin dimethyl ester. The revised assignments are shown in Figure 3. Further comparisons of the spectra are as follows: (i) the resonance of C^5 or C^{10} (102.3 ppm average) of bonellin, each of which is flanked by a single β-alkyl substituent, is shifted upfield by 4.4 ppm compared to that of $\mathbf{H_2C}$. This upfield shift can be explained by the substituent effect of a β-alkyl group on the chemical shifts of *meso*-carbons as described above. The resonance of C^5 (=C^{10}, 98.3 ppm[19]) of $\mathbf{H_2OEC}$, which is flanked by two β-alkyl substituents, is shifted upfield by 8.4 ppm compared to that of $\mathbf{H_2C}$. Thus, the presence of one alkyl substituent adjacent to a *meso*-position causes a ~4 ppm downfield shift of the resonance of the *meso*-carbon. (ii) The chemical shifts of β-pyrrole carbons can be easily explained by the α-effect of alkyl substitution (e.g., the methyl group causes a 9.3 ppm downfield shift[27]). (iii) The chemical shifts of α-pyrrole carbons are closely matched in $\mathbf{H_2C}$ and bonellin dimethyl ester.

(b) **ZnC** versus **13²(*R*)-Chl *a***: there are several discrepancies between the chemical shifts of **ZnC** and those of **13²(*R*)-Chl *a*** that do not stem from the different metalation states (zinc vs magnesium). The largest discrepancies are observed for the following carbons: (i) C^6; 146.4 ppm ($\mathbf{H_2C}$) versus 152.7 ppm (**13²(*R*)-Chl *a***). The effect of β-substitution on the chemical shift of the α-carbon is very small. The chemical shift of the resonance of C^6 of **13²(*R*)-Chl *a*** should be similar to that of C^9 of **13²(*R*)-Chl *a*** (~146 ppm). (ii) C^7; 132.2 ppm ($\mathbf{H_2C}$) versus 134.0 ppm (**13²(*R*)-Chl *a***). Upon considering the expected α-effect of the 7-methyl group (~9.3 ppm downfield shift[27]), the resonance of C^7 should appear near 140 ppm. (iii) C^{10}; 107.9 ppm ($\mathbf{H_2C}$) versus 108.2 ppm (**13²(*R*)-Chl *a***). The chemical shift of the resonance from C^{10} of **13²(*R*)-Chl *a*** should be similar to that of **MgOEC** (~101 ppm[20]). Indeed, there are many reports of chlorophyll analogues wherein a resonance at ~100 ppm is assigned to C^{10}.[28–34] These discrepancies might be attributed to the presence of the isocyclic ring in **13²(*R*)-Chl *a***. Further studies using chlorin benchmarks containing an isocyclic ring are required to resolve such apparent discrepancies.

2.3. Absorption and fluorescence properties

2.3.1. Comparison of spectral features of chlorin benchmarks. The fully unsubstituted chlorins $\mathbf{H_2C}$, **MgC**, and **ZnC** exhibit absorption and fluorescence spectral features similar to those of the corresponding derivatives of chlorin itself (**H_2Chlorin**, **MgChlorin**, and **ZnChlorin**), where data are available (Table 4). On the other hand, the synthetic chlorins prepared herein lack auxochromes at the 3- and 13-positions, which accentuate the long-wavelength transition of chlorophylls (which contain a 3-vinyl group and a 13-keto group).[7] Hence the spectra of the synthetic chlorins typically exhibit less red absorption than the chlorophylls. The availability of the synthetic chlorins enables these differences to be probed in detail.

Table 4. Spectral properties of chlorins[a]

Compound	λ_B in nm (log ε)	λ_{Q_y} in nm (log ε)	I_B/I_Q[b]	λ_{em} in nm	Φ_f[c]
H_2C	389 (5.20)	634 (4.82)	2.4	636	0.19
H_2Chlorin	388 (5.11)[d]	638 (4.70)[d]	2.6	—	0.20[e]
Pheo *a*	409 (5.06)[f]	667 (4.74)[f]	2.1	—	0.175[g]
MgC	402 (5.35)	607 (4.65)	4.4	610	0.26
MgChlorin	402 (5.49)[h]	610 (4.75)[h]	5.5	—	—
Chl *a*	429 (5.05)[i]	661 (4.94)[i]	1.3	666[j]	0.325[g]
ZnC[k]	399 (5.38)	603 (4.84)	3.5	605	0.062
ZnChlorin	402[l]	603[l]	3.6	—	—
Zn-Pheo *a*	423 (5.09)[m]	653 (4.96)[m]	1.4	657	0.23
Oxo-ZnC	412 (5.19)	602 (4.65)	3.5	605	0.026[n]
PdC	390	586	1.7	—	—
CuC	397	596	3.9	—	—

[a] In toluene at room temperature unless noted otherwise.
[b] Ratio of the intensity of the B and Q_y bands.
[c] Each Φ_f value was determined in toluene at room temperature with λ_{exc} at the B band maximum using chlorophyll *a* as a standard (Φ_f=0.322) unless noted otherwise (see text).
[d] Ref. 5 (in benzene).
[e] Ref. 36 (in propanol).
[f] Ref. 37 (in diethyl ether).
[g] Ref. 38 (in benzene).
[h] Ref. 5 (in benzene).
[i] Ref. 35 (in diethyl ether).
[j] Ref. 39.
[k] Ref. 7.
[l] Ref. 40 (in *n*-octane).
[m] Ref. 41 (in diethyl ether).
[n] Ref. 42 (in diethyl ether).

An example of the difference in absorption spectra is provided by **H_2C** and pheophorbide *a*, the free base and dephytylated analogue of chlorophyll *a* (**Pheo *a***), as is shown in Figure 4. The ratio of the intensity of the B and Q_y bands (I_B/I_Q ratio),[35] which provides a measure of the relative amount of blue:red absorption, is greater for the synthetic chlorins than the chlorophylls. The most pronounced difference occurs in the magnesium chelates, where **MgC** exhibits an I_B/I_Q ratio of 4.4 versus 1.3 for that of chlorophyll *a*.

The fluorescence quantum yields of the synthetic chlorins can be compared with those of other chlorins, including chlorophyll and its metalated analogues. The fluorescence quantum yield of **H_2C** is nearly identical with that of **Pheo *a*** (Φ_f=0.19 vs 0.175), the yields for **MgC** and chlorophyll *a* are similar (0.26 vs 0.325), but a sizable disparity occurs for **ZnC** and **Zn-Pheo *a*** (0.062 vs 0.23). The zinc-oxochlorins (**Oxo-ZnC**, **Oxo-ZnC-B**[5]) exhibit even lower fluorescence yields (0.026, 0.029). The fluorescence quantum yield for **H_2C** is nearly identical with that for **H_2Chlorin** (Φ_f=~0.20). To our knowledge, fluorescence yield data are not available for **MgChlorin** and **ZnChlorin**.

Thus, the geminal dimethyl-substituted chlorins exhibit spectral attributes resembling those of the less stable analogues that have been prepared previously. The availability of diverse synthetic chlorins enables a number of spectral studies. The comparisons presented here concern the effects of core modification (metalation, protonation) and the effects of increasing number of *meso*-substituents in free base chlorins.

2.3.2. Absorption spectra of metallochlorins. The absorption spectra of several metallochlorins (**ZnC**, **CuC**, **MgC**, and **PdC**)[2] are shown in Figure 5. The absorption spectra of **CuC**, **MgC**, and **ZnC** exhibit the following characteristic features: (i) blue shift of the Q_y band (27–38 nm) compared to **H_2C**, (ii) narrower B band (fwhm=10–13 nm) compared to **H_2C** (fwhm=33 nm), (iii) larger I_B/I_Q ratio (3.5–4.4) compared to **H_2C** (2.4). **PdC** shows the following distinctive features versus **ZnC**: (i) a further blue shift of the Q_y band (17 nm), (ii) broadening of the B band (fwhm=26 nm), and (iii) a smaller I_B/I_Q ratio (1.7).

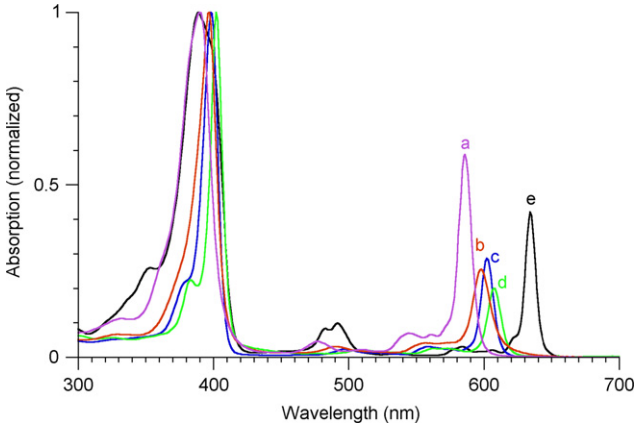

Figure 5. Absorption spectra of metallochlorins in toluene at room temperature. Legend: **PdC** (a, purple), **CuC** (b, red), **ZnC** (c, blue), **MgC** (d, green), and **H_2C** (e, black).

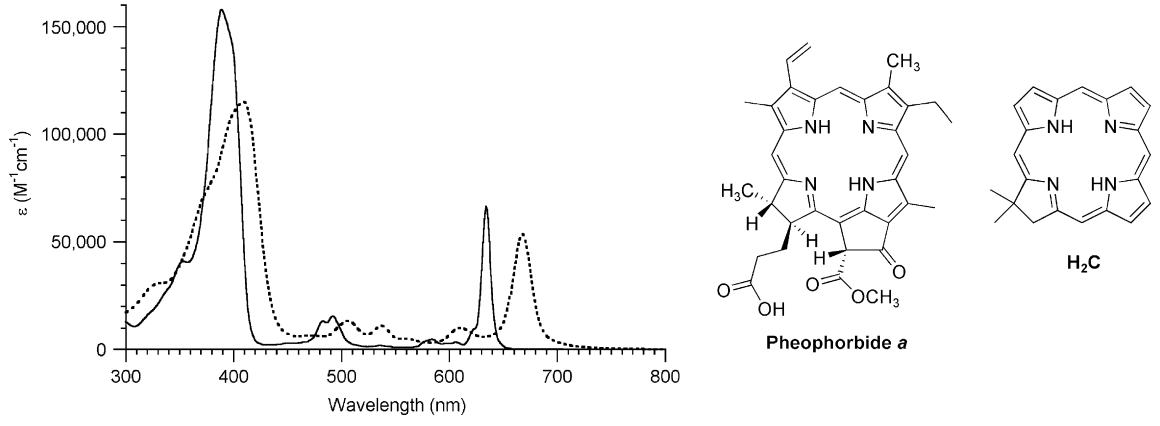

Figure 4. Absorption spectra of **H_2C** (solid line, in toluene) and **Pheo *a*** (dashed line, in diethyl ether).

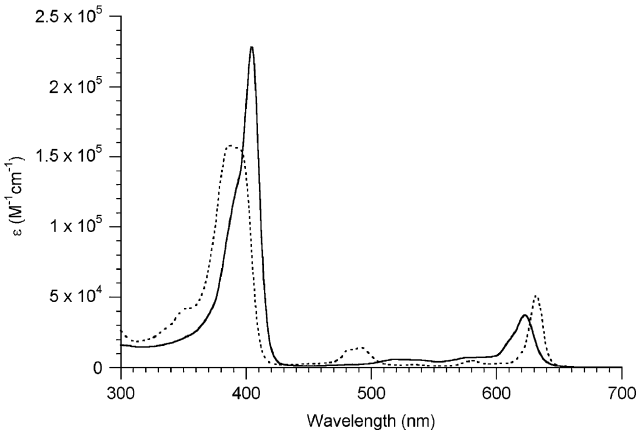

Figure 6. Absorption spectra at room temperature of $\mathbf{H_2C}$ (dashed line) in toluene and putative $\mathbf{H_4C^{2+}}$ (solid line) in acidified toluene.

2.3.3. Absorption spectra of protonated chlorins. A solution of $\mathbf{H_2C}$ in toluene upon treatment with TFA (~1% v/v) underwent protonation to form the putative $\mathbf{H_4C^{2+}}$. The absorption spectrum is shown in Figure 6. The chlorin dication exhibits a red shifted B band [$\mathbf{H_2C}$, 388 nm (log ε=5.20); $\mathbf{H_4C^{2+}}$, 404 (log ε=5.45)] and slightly blue shifted Q_y band [$\mathbf{H_2C}$, 632 nm (log ε=4.71); $\mathbf{H_4C^{2+}}$: 623 nm (log ε=4.57)]. The disubstituted chlorin $\mathbf{H_2C\text{-}T^5M^{10}}$ (λ_B=414 nm, log ε_B=4.95; λ_Q=641 nm, log ε_Q=4.45) upon diprotonation exhibited similar spectral shifts (λ_B=425 nm, log ε_B=5.06; λ_Q=622 nm, log ε_Q=4.09). In each case the spectrum of the free base chlorin was reobtained upon neutralization with triethylamine. Similar features were observed with the diprotonated tetraphenylchlorin ($\mathbf{H_4TPC^{2+}}$).[3]

2.3.4. Absorption spectra of *meso*-aryl-substituted free base chlorins. The absorption spectra of free base chlorins with 0–3 substituents are displayed in Figure 7 and summarized in Table 5. The B band and Q_y band of the free base *meso*-substituted chlorins are steadily red shifted with increasing number of aryl substituents from 0 to 3, while the I_B/I_Q ratio increases from 2.4 (unsubstituted) to 3.8 (trisubstituted). The following observations concern the additive effects of *meso*-aryl groups giving rise to the red shift for both the B and Q_y bands: (i) the Q_y band of chlorins is red

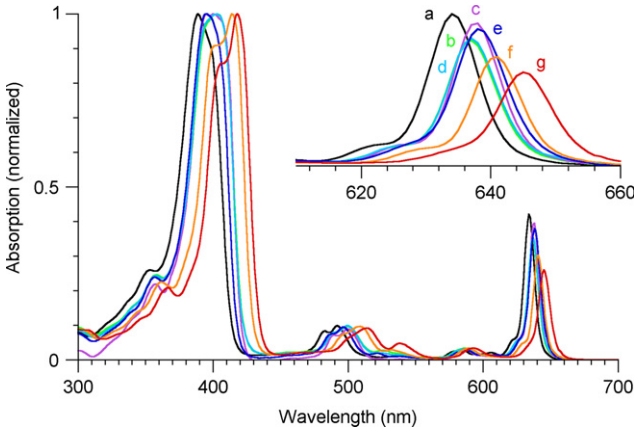

Figure 7. Absorption spectra of free base chlorins with 0–3 *meso*-substituents in toluene at room temperature. Legend: $\mathbf{H_2C}$ (a, black), $\mathbf{H_2C\text{-}T^5}$ (b, green) $\mathbf{H_2C\text{-}M^{10}}$ (c, purple), $\mathbf{H_2C\text{-}P^{10}}$ (d, light blue), $\mathbf{H_2C\text{-}P^{15}}$ (e, blue), and $\mathbf{H_2C\text{-}T^5M^{10}}$ (f, yellow), and $\mathbf{H_2C\text{-}T^5M^{10}P^{15}}$ (g, red).

Table 5. Spectral properties of free base chlorins with 0–3 substituents[a]

Number of substituents	Compound	λ_B (nm)	$\Delta\lambda_B$[b] (nm)	λ_{Q_y} (nm)	$\Delta\lambda_{Q_y}$[b] (nm)	I_B/I_Q[c]
0	$\mathbf{H_2C}$	389	—	634	—	2.4
1	$\mathbf{H_2C\text{-}T^5}$	403	+14	637	+3	2.9
1	$\mathbf{H_2C\text{-}M^{10}}$	400	+11	638	+4	2.5
1	$\mathbf{H_2C\text{-}P^{10}}$	403	+14	637	+3	2.8
1	$\mathbf{H_2C\text{-}P^{15}}$	395	+6	638	+4	2.6
2	$\mathbf{H_2C\text{-}T^5M^{10}}$	414	+25	641	+7	3.3
2	$\mathbf{H_2C\text{-}P^{10}P^{15}}$	408	+19	641	+7	3.1
3	$\mathbf{H_2C\text{-}T^5M^{10}P^{15}}$	418	+29	645	+11	3.8

[a] In toluene at room temperature unless noted otherwise.
[b] Shift in peak wavelength from that of $\mathbf{H_2C}$.
[c] Ratio of the intensity of the B and Q_y bands.

shifted ~4 nm by the introduction of each *meso*-aryl substituent regardless of the type or position of the substituent. This effect was additive, giving a total red shift of ~11 nm for the Q_y band of the triaryl-substituted chlorin $\mathbf{H_2C\text{-}T^5M^{10}P^{15}}$. (ii) The magnitude of the red shift of the B band depends on both the type and position of the substituents: 5-position (14 nm for *p*-tolyl), 10-position (14 nm for phenyl, 11 nm for mesityl), and 15-position (6 nm for phenyl). The magnitude of the red shift for multiple *meso*-aryl-substituted chlorins can be calculated by adding these numbers (e.g., $\mathbf{H_2C\text{-}T^5M^{10}}$, calculated red shift 25 nm (14+11 nm), observed 25 nm; $\mathbf{H_2C\text{-}P^{10}P^{15}}$, calculated red shift 20 nm (14+6 nm), observed 19 nm; $\mathbf{H_2C\text{-}T^5M^{10}P^{15}}$, calculated red shift 31 nm (14+11+6 nm), observed 29 nm).

Spectral trends similar to those described herein for chlorins also have been observed with porphyrins. Senge and coworkers reported absorption spectra of porphyrins that bear 1–4 *meso*-aryl substituents[43] and noted a continual red shift of the absorption spectra with increasing number of aryl substituents. The correlation between the number of substituents and the ratio of the intensity of the Soret band and that of the dominant visible band (I_B/I_Q ratio) should also be noted: the I_B/I_Q ratio increases from 14.7 in porphine to 50 in tetramesitylporphyrin due to the four aryl substituents (on the basis of data from Ref. 39).

A deep understanding of the origin of the differences in spectral attributes and fluorescence yields will require additional spectroscopic and other physical studies. Such studies are now possible given the availability of the benchmark chlorins described herein as well as analogous chlorins bearing substituents at designated locations.

2.4. X-ray crystal structures

More than 75 crystal structures of chlorins have been reported.[44] To our knowledge, however, there are no reported X-ray crystal structures of a chlorin lacking any substituents at the *meso*- and β-pyrrolic positions, nor are there crystal structures of chlorins possessing relatively few (1–3) substituents. The typical synthetic chlorins that have been examined by X-ray crystallography contain a full complement of aryl or alkyl substituents at the *meso*- or β-positions. Moreover, only a few crystal structures of oxochlorins have been reported, and these are for the iron or nickel chelate.[45]

Single crystals of unsubstituted chlorin (**ZnC**) and unsubstituted oxochlorin (**Oxo-ZnC**) were grown from dichloromethane/cyclohexane and subjected to X-ray crystallographic analysis. Key structural parameters are listed in Table 6.

ORTEP drawings of **ZnC** and **Oxo-ZnC** are shown in Figure 8 together with the bond distances. The carbon–carbon bond lengths in the pyrroline ring (ring D) are distinct from those in three pyrrole rings due to the sp^3 versus sp^2 hybridization. In **ZnC**, for example, the C17–C18 distance (1.507 Å) or the C16–C17 distance (1.500 Å) is longer than the average of the corresponding bond distances in the pyrrole rings (1.340 or 1.434 Å, respectively). The distances between the zinc atom and the four nitrogen atoms resemble those of other chlorins. The distance between the zinc atom to the pyrroline nitrogen atom (2.103 Å for **ZnC** and 2.098 Å for **Oxo-ZnC**) in each case is longer than that between the zinc atom and a pyrrole nitrogen atom by ~0.04 to ~0.09 Å. Similar observations were reported for other metallochlorins (e.g., **ZnTPC**,[46] **PdOEC**,[47] **FeOEC**,[48] **NiTMC**[49]). The core size (pairwise distances between the four nitrogen atoms N1–N2, N2–N3, N3–N4, N4–N1) of **ZnC**, **Oxo-ZnC**, and **ZnTPC**[46] give values that are similar to each other, with average nitrogen–nitrogen distances of 2.896, 2.908, and 2.906 Å, respectively. In each molecule, the N3–N4 and N4–N1 distances are slightly longer (~0.03 Å) than those for N1–N2 and N2–N3.

The distances of atoms in the chlorin macrocycle from their least-squares plane (24 non-hydrogen atoms) are listed in Figure 9. The degree of distortion of the macrocycle (calculated by the sum of the averaged positive displacement and the averaged negative displacement) is nearly identical for **ZnC** (0.122 Å) and **Oxo-ZnC** (0.119 Å). The largest deviation was observed for C18 of **Oxo-ZnC**, which is out-of-plane by 0.256 Å. This is mainly due to relief of strain in the pyrroline ring owing to the adjacent 17-oxo group. The zinc atom is displaced 0.219 and 0.152 Å out-of-plane in **ZnC** and **Oxo-ZnC**, respectively. These displacements are significantly less than that in **ZnTPC**, where the zinc atom is displaced 0.39 Å out-of-plane.[46] The latter molecule may be somewhat more strained owing to the two *meso*-phenyl groups flanking the pyrroline ring.

ZnC and **Oxo-ZnC** crystallized with inclusion of cyclohexane in the unit cell (**ZnC**:cyclohexane=2:1; **Oxo-ZnC**:cyclohexane=1:1). Each unit cell of **ZnC** contains

Table 6. Summary of crystal data for **ZnC** and **Oxo-ZnC**

	ZnC+0.5 cyclohexane	**Oxo-ZnC**+cyclohexane
Formula	$C_{25}H_{24}N_4Zn$	$C_{28}H_{28}N_4OZn$
Formula weight (g/mol)	445.87	501.91
Crystal dimensions (mm)	0.34×0.16×0.01	0.30×0.14×0.04
Crystal color and habit	Purple plates	Purple plates
Crystal system	Monoclinic	Monoclinic
Space group	*C*2/*c*	$P2_1/c$
Temperature (K)	110	110
a (Å)	27.186 (3)	15.4858 (14)
b (Å)	12.2685 (14)	13.5067 (11)
c (Å)	12.0438 (14)	11.5020 (9)
α (°)	90.0	90.00
β (°)	93.878 (4)	98.838 (4)
γ (°)	90.0	90.00
V (Å^3)	4007.8 (8)	2377.2 (3)
Number of reflections to determine final unit cell	7067	7685
2θ for cell determination (°)	$5.60<2\theta<53.48$	$5.10<2\theta<50.06$
Index range	$-34\le h\le 34$	$-18\le h\le 18$
	$0\le k\le 15$	$-16\le k\le 15$
	$0\le l\le 15$	$-13\le l\le 13$
Z	8	4
F(000)	1859.40	1048
ρ (g/cm)	1.478	1.402
λ (Å, Mo Kα)	0.71073	0.71073
μ (cm^{-1})	1.25	1.062
Scan type(s)	Omega and phi scans	Omega and phi scans
Max 2θ for data collection (°)	53.60	50.2
Measured fraction of data		0.992
Number of reflections measured	25,380	133,290
Unique reflections measured	4287	4216
R_{merge}	0.034	0.0516
Structure refined using	Full matrix least-squares based on *F*	Full matrix least-squares using F^2
Weighting scheme	Sigma[a]	Calcd[b]
Number of parameters in least-squares	271	309
Final *R* indices	*R*=0.063	*R*=0.0819
	Rw=0.070	*Rw*=0.2274
R indices (all data)	*R*=0.074	*R*=0.0986
	Rw=0.071	*Rw*=0.2455
GOF	2.23	1.015
Maximum shift/error	0.000	0.000
Min and max peak heights on final ΔF map (e$^-$/Å)	−0.82, 2.22	−0.788, 4.770

[a] $w=1/[\text{sigma}^2F+0.004F^2]$.
[b] $w=1/[\text{sigma}^2(F_0^2)+(0.1485P)^2+10.9233P]$, where $P=(F_0^2+2F_c^2)/3$.

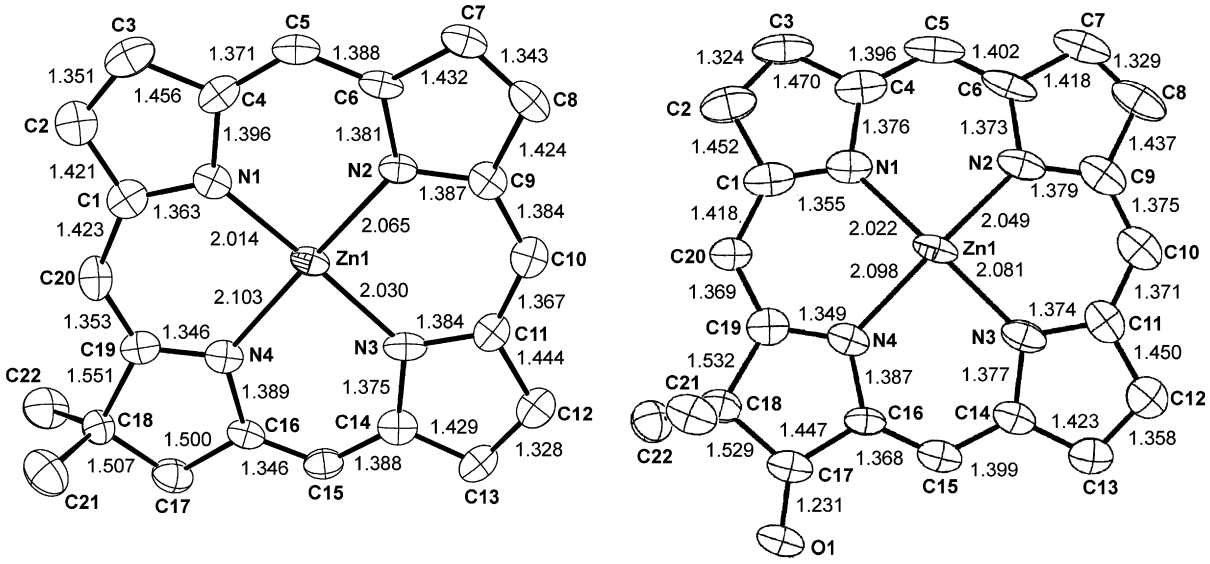

Figure 8. Projection view of **ZnC** (left) and **Oxo-ZnC** (right) showing bond distances. The thermal ellipsoids are drawn at the 50% probability level. Hydrogen atoms are omitted for clarity. Estimated standard deviations on bond distances are 0.002–0.005 Å.

eight chlorin molecules and four cyclohexane molecules, whereas each unit cell of **Oxo-ZnC** contains four chlorin molecules and four cyclohexane molecules. The molecular packing patterns in the unit cell of **ZnC** (left) and **Oxo-ZnC** (right) are shown in Figure 10. The **ZnC** macrocycles are arranged as slipped cofacial dimers without any apical ligand at the zinc site; each zinc atom is tetracoordinate with a very slight out-of-plane distortion from square planar geometry. The presence of the 17-oxo group profoundly changes the packing pattern. The **Oxo-ZnC** macrocycles are arranged in a polymeric network owing to coordination of the carbonyl oxygen atom of one oxochlorin to the apical zinc atom of an adjacent oxochlorin. Each oxochlorin in a given polymer also forms a cofacial interaction with an oxochlorin in a neighboring polymer.

Greater insight into the stacking is provided in Figure 11. In **ZnC**, the cofacial interaction entails opposite faces of the two macrocycles, with rings A and C (B and D) of one chlorin juxtaposed against rings C and A (D and B), respectively, of the facing chlorin (see Chart 2 for ring labels and recall that the **ZnC** molecule has C_s symmetry). The two macrocycles are laterally offset by 2.0 Å along the axis that bisects the nitrogen atoms of rings B and D, with no offset along the axis that bisects the nitrogen atoms of rings A and C. Such offset positions the geminal dimethyl groups outside the region of cofacial overlap, and the pairing of opposite faces gives an anti-type relationship of the respective geminal dimethyl groups. Thus, the nitrogen atom of ring D of a given chlorin projects over the midpoint of the β,β′-bond of pyrrole ring B of the facing chlorin. Such π−π interaction is typical for a variety of porphyrinic macrocycles.[50] The shortest contact between two chlorin molecules in **ZnC** is 2.827 Å, which occurs between the zinc atom of one chlorin molecule and an inner nitrogen (N2) of the other chlorin molecule. Although this distance is short, both the zinc atom and the nitrogen atom lie toward each other, very slightly (~0.2 Å each) out of their respective macrocycle planes. The distance between least-squares planes (~3.2 Å) is shorter than typical for porphyrinic macrocycles that bear peripheral substituents, but is comparable to that observed in the nickel chelate of porphine [porphinatonickel(II), 3.355 Å], which also lacks sterically encumbering peripheral substituents.[51]

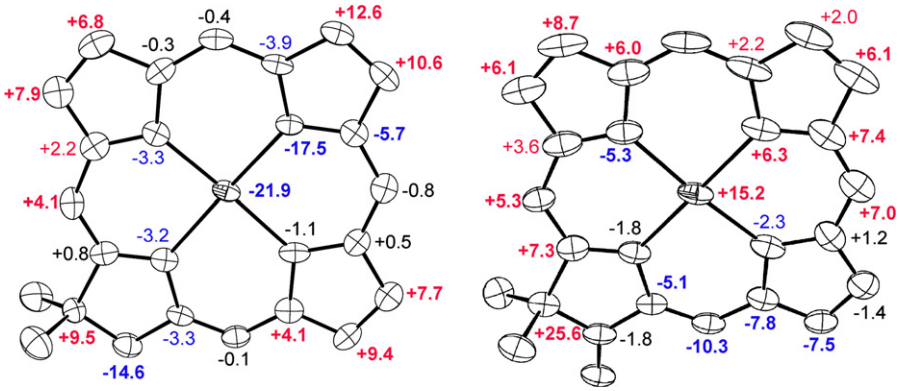

Figure 9. Deviations of the carbon atoms in **ZnC** (left) and **Oxo-ZnC** (right) from the least-squares plane of the chlorin macrocycle (Å×10^2). Hydrogen atoms are omitted for clarity.

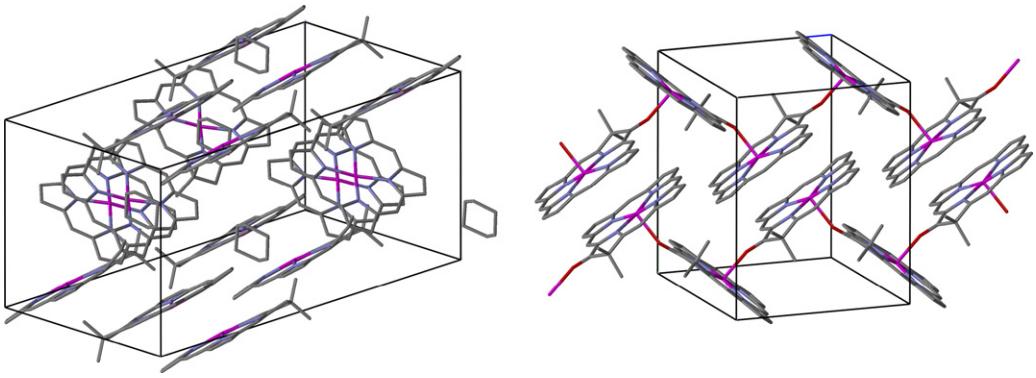

Figure 10. View of the molecular packing diagram of **ZnC** (left) and **Oxo-ZnC** (right). In the diagram for **Oxo-ZnC**, solvent molecules are omitted for clarity.

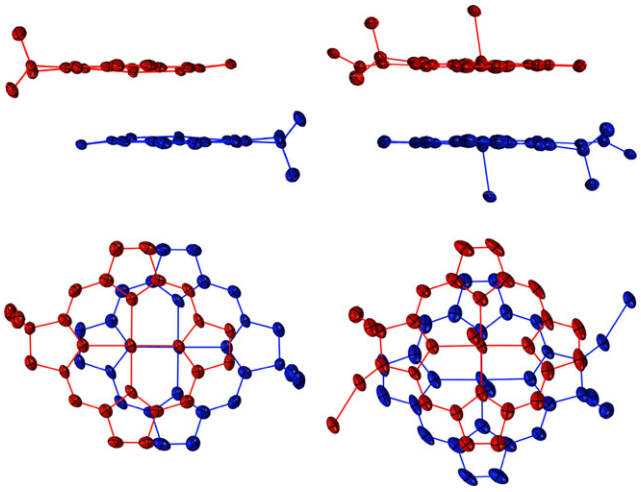

Figure 11. Views of the stacking of **ZnC** (left) and **Oxo-ZnC** (right).

In **Oxo-ZnC**, the cofacial interaction also entails opposite faces of the two macrocycles. However, the lateral offset (by 1.5 Å) occurs along the axis that bisects the nitrogen atoms of rings A and C, with no offset along the axis that bisects the nitrogen atoms of rings B and D. Such pairing of opposite faces and lateral offset also positions the geminal dimethyl groups in an *anti*-configuration outside of the region of cofacial overlap. Thus, the two α-carbon atoms of pyrrole ring A of a given chlorin overlap with the two β-carbon atoms of pyrrole ring C of the facing chlorin. The distance between a zinc atom and the ligated carbonyl atom is 2.248 Å, which is the shortest contact between two neighboring oxochlorin molecules. The closest cofacial approach of two atoms is 3.230 Å (C^{13} of one macrocycle and C^{4} of the facing macrocycle). The π−π interaction in **Oxo-ZnC** remains significant, albeit less than that in **ZnC**, given the slightly longer average interplanar distance in the oxochlorin (∼3.3 Å) versus the chlorin (∼3.2 Å).

3. Conclusions

The unsubstituted chlorins (**H_2C**, **ZnC**), oxochlorin (**Oxo-ZnC**), and sparsely substituted analogues constitute benchmark macrocycles against which more complex hydroporphyrins can be compared. The absorption spectral data provide quantitative reference points for understanding how substituents alter electronic properties and shift spectral bands. The ^{1}H NMR and ^{13}C NMR data may prove useful for characterizing more highly substituted chlorins. The X-ray data may establish the foundation for studies of crystal engineering, where substituents are employed to alter crystal-packing patterns and elicit desirable photophysical and electronic features.

4. Experimental section

4.1. General methods

^{1}H NMR (400 MHz) and ^{13}C NMR (100 MHz) spectra were collected at room temperature in $CDCl_3$ unless noted otherwise. Absorption and fluorescence spectra were obtained in toluene at room temperature.

4.2. Molar absorption coefficients

Molar absorption coefficients were calculated through use of the Beer–Lambert law ($A=\varepsilon\times c\times l$). The absorption spectrum of a chlorin was recorded at room temperature in toluene maintaining the intensity of the absorption maximum (B band, 389–412 nm) within the range of 0.8–1.2. A typical procedure is as follows: (1) a known quantity of the chlorin [e.g., 19.3 mg (56.7 μmol) of **H_2C**] was dissolved in 25 mL of toluene (spectroscopic grade) using a 25 mL volumetric flask. (2) A 1.00-mL aliquot of this solution was removed and diluted with toluene in a 25 mL volumetric flask (25 times dilution). (3) A known quantity (typically ∼1 mL, 0.600 mL for **H_2C**) of this solution was removed and diluted with toluene in a 10 mL volumetric flask (∼10 times dilution). (4) This solution was placed in a 1-cm pathlength cuvette, and the absorption spectrum was recorded. The absorption spectrometer was a diode array instrument with resolution of 1 nm.

The molar absorption coefficient for **MgC** in toluene was initially determined as ε_{402nm}=159,000 $M^{-1}\,cm^{-1}$ and ε_{611nm}=32,100 $M^{-1}\,cm^{-1}$. However, ^{1}H NMR spectroscopy (in C_6D_6) of the same sample of **MgC** revealed the presence of H_2O (∼six molecules of H_2O per molecule of **MgC**, after taking into account the background H_2O in the NMR solvent) and THF (∼one molecule of THF per two molecules of **MgC**) attributed at least in part to association with magnesium. We could not remove such solvent molecules from

the sample despite prolonged drying under high vacuum. Therefore, the corrected values for the molar absorption coefficients in toluene are ε_{402nm}=220,000 $M^{-1}\,cm^{-1}$ (log ε=5.34) and ε_{611nm}=45,000 $M^{-1}\,cm^{-1}$ (log ε=4.65).

4.3. Fluorescence quantum yields (Φ_f)

The Φ_f values for the chlorins were determined with chlorin samples in toluene at room temperature as described previously (see Supporting Information of Ref. 7) using chlorophyll *a* as the standard (Φ_f=0.325 in benzene),[38] which gives Φ_f=0.322 in toluene.

4.4. X-ray crystallographic analysis of chlorins

4.4.1. Data collection and processing. The samples were mounted on a nylon loop with a small amount of NVH immersion oil. All X-ray measurements were made on a Bruker-Nonius X8 Apex2 CCD diffractometer at 110 K. The frame integration was performed using SAINT+.[52] The resulting raw data were scaled and absorption-corrected by multi-scan averaging of symmetry equivalent data using SADABS.[53]

4.4.2. Structure solution and refinement. The structures were solved by direct methods using SIR92.[54] All non-hydrogen atoms were obtained from the initial E-map. The hydrogen atoms were placed at idealized positions and were allowed to ride on the parent carbon atom. The structural model was fit to the data using full matrix least-squares based on F (for **ZnC**) or F^2 (for **Oxo-ZnC**). The calculated structure factors included corrections for anomalous dispersion from the usual tabulation. The structure was refined using the XL program from the SHELXTL package,[55] and graphic plots were produced using the version of ORTEP included in the NRCVAX crystallographic program suite.[56]

Acknowledgements

This work was supported by the NIH (GM36238). Mass spectra were obtained at the Mass Spectrometry Laboratory for Biotechnology at North Carolina State University. Partial funding for the facility was obtained from the North Carolina Biotechnology Center and the NSF.

References and notes

1. Ptaszek, M.; McDowell, B. E.; Taniguchi, M.; Kim, H.-J.; Lindsey, J. S. *Tetrahedron* **2007**, *63*, 3826–3839.
2. Taniguchi, M.; Ptaszek, M.; McDowell, B. E.; Lindsey, J. S. *Tetrahedron* **2007**, *63*, 3840–3849.
3. Dorough, G. D.; Huennekens, F. M. *J. Am. Chem. Soc.* **1952**, *74*, 3974–3976.
4. Eisner, U. *J. Chem. Soc.* **1957**, 3461–3469.
5. Eisner, U.; Linstead, R. P. *J. Chem. Soc.* **1955**, 3742–3749.
6. Egorova, G. D.; Solov'ev, K. N.; Shul'ga, A. M. *J. Gen. Chem. USSR* **1967**, *37*, 333–336.
7. Laha, J. K.; Muthiah, C.; Taniguchi, M.; McDowell, B. E.; Ptaszek, M.; Lindsey, J. S. *J. Org. Chem.* **2006**, *71*, 4092–4102.
8. Taniguchi, M.; Ra, D.; Mo, G.; Balasubramanian, T.; Lindsey, J. S. *J. Org. Chem.* **2001**, *66*, 7342–7354.
9. Strachan, J.-P.; O'Shea, D. F.; Balasubramanian, T.; Lindsey, J. S. *J. Org. Chem.* **2000**, *65*, 3160–3172.
10. Taniguchi, M.; Kim, M. N.; Ra, D.; Lindsey, J. S. *J. Org. Chem.* **2005**, *70*, 275–285.
11. Taniguchi, M.; Kim, H.-J.; Ra, D.; Schwartz, J. K.; Kirmaier, C.; Hindin, E.; Diers, J. R.; Prathapan, S.; Bocian, D. F.; Holten, D.; Lindsey, J. S. *J. Org. Chem.* **2002**, *67*, 7329–7342.
12. Smith, K. M.; Goff, D. A.; Abraham, R. J.; Plant, J. E. *Org. Magn. Reson.* **1983**, *21*, 505–511.
13. Solov'ev, K. N.; Mashenkov, V. A.; Gradyushko, A. T.; Turkova, A. E.; Lezina, V. P. *Zh. Prikl. Specktr.* **1970**, *13*, 339–345 (Eng. Translation, pp 1106–1111).
14. Kozlowski, P. M.; Wolinski, K.; Pulay, P.; Ye, B.-H.; Li, X.-Y. *J. Phys. Chem. A* **1999**, *103*, 420–425.
15. Bonnett, R.; Djelal, B. D.; Hawkes, G. E.; Haycock, P.; Pont, F. *J. Chem. Soc., Perkin Trans. 2* **1994**, 1839–1843.
16. Shulga, A. M.; Sinyakov, G. N.; Filatov, I. V.; Gurinovich, G. P.; Dzilinski, K. *Biospectroscopy* **1995**, *1*, 223–234.
17. Neya, S.; Quan, J.; Hoshino, T.; Hata, M.; Funasaki, N. *Tetrahedron Lett.* **2004**, *45*, 8629–8630.
18. Kilpeläinen, I.; Kaltia, S.; Kuronen, P.; Hyvärinen, K.; Hynninen, P. H. *Magn. Reson. Chem.* **1994**, *32*, 29–35.
19. Smith, K. M.; Unsworth, J. F. *Tetrahedron* **1975**, *31*, 367–375.
20. Stolzenberg, A. M.; Stershic, M. T. *Inorg. Chem.* **1987**, *26*, 1970–1977.
21. Ulman, A. *Org. Magn. Reson.* **1984**, *22*, 114–116.
22. Stolzenberg, A. M.; Stershic, M. T. *Magn. Reson. Chem.* **1987**, *25*, 256–259.
23. Hynninen, P. H.; Helaja, J.; Montforts, F.-P.; Müller, C. M. *J. Porphyrins Phthalocyanines* **2004**, *8*, 1376–1382.
24. Sugiura, K.-I.; Ponomarev, G.; Okubo, S.; Tajiri, A.; Sakata, Y. *Bull. Chem. Soc. Jpn.* **1997**, *70*, 1115–1123.
25. Balasubramanian, T.; Strachan, J. P.; Boyle, P. D.; Lindsey, J. S. *J. Org. Chem.* **2000**, *65*, 7919–7929.
26. Hyvärinen, K.; Helaja, J.; Kuronen, P.; Kilpeläinen, I.; Hynninen, P. H. *Magn. Reson. Chem.* **1995**, *33*, 646–656.
27. Ewing, D. E. *Org. Magn. Reson.* **1979**, *12*, 499–524.
28. Smith, K. M.; Goff, D. A. *J. Chem. Soc., Perkin Trans. 1* **1985**, 1099–1113.
29. Timkovich, R.; Bondoc, L. L. *Magn. Reson. Chem.* **1989**, *27*, 1048–1051.
30. Helaja, J.; Tauber, A. Y.; Kilpeläinen, I.; Hynninen, P. H. *Magn. Reson. Chem.* **1997**, *35*, 619–628.
31. Cheng, H.-H.; Wang, H.-K.; Ito, J.; Bastow, K. F.; Tachibana, Y.; Nakanishi, Y.; Xu, Z.; Luo, T.-Y.; Lee, K.-H. *J. Nat. Prod.* **2001**, *64*, 915–919.
32. Sobolev, A. P.; Brosio, E.; Gianferri, R.; Segre, A. L. *Magn. Reson. Chem.* **2005**, *43*, 625–638.
33. Hynninen, P. H.; Leppäkases, T. S.; Mesilaakso, M. *Tetrahedron* **2006**, *62*, 3412–3422.
34. Hynninen, P. H.; Leppäkases, T. S.; Mesilaakso, M. *Tetrahedron Lett.* **2006**, *47*, 1663–1668.
35. Strain, H. H.; Thomas, M. R.; Katz, J. J. *Biochim. Biophys. Acta* **1963**, *75*, 306–311.
36. Gradyushko, A. T.; Sevchenko, A. N.; Solovyov, K. N.; Tsvirko, M. P. *Photochem. Photobiol.* **1970**, *11*, 387–400.
37. Smith, J. H. C.; Benitez, A. *Modern Methods of Plant Analysis*; Paech, K., Tracey, M. V., Eds.; Springer: Berlin, 1955; Vol. IV, pp 142–196.
38. Weber, G.; Teale, F. W. J. *Trans. Faraday Soc.* **1957**, *53*, 646–655.
39. Dixon, J. M.; Taniguchi, M.; Lindsey, J. S. *Photochem. Photobiol.* **2005**, *81*, 212–213.

40. Singh, A.; Johnson, L. W. *Spectrochim. Acta Part A* **2002**, *58*, 1573–1576.
41. Jones, I. D.; White, R. C.; Gibbs, E.; Denard, C. D. *J. Agric. Food Chem.* **1968**, *16*, 80–83.
42. Agostiano, A.; Catucci, L.; Colafemmina, G.; Scheer, H. *J. Phys. Chem. B* **2002**, *106*, 1446–1454.
43. Ryppa, C.; Senge, M. O.; Hatscher, S. S.; Kleinpeter, E.; Wacker, P.; Schilde, U.; Wiehe, A. *Chem.—Eur. J.* **2005**, *11*, 3427–3442.
44. Senge, M. O. *The Porphyrin Handbook*; Kadish, K. M., Smith, K. M., Guilard, R., Eds.; Academic: San Diego, CA, 2000; Vol. 10, pp 1–218.
45. (a) Stolzenberg, A. M.; Glazer, P. A.; Foxman, B. M. *Inorg. Chem.* **1986**, *25*, 983–991; (b) Connick, P. A.; Haller, K. J.; Macor, K. A. *Inorg. Chem.* **1993**, *32*, 3256–3264; (c) Cai, S.; Belikova, E.; Yatsunyk, L. A.; Stolzenberg, A. M.; Walker, F. A. *Inorg. Chem.* **2005**, *44*, 1882–1889.
46. Spaulding, L. D.; Andrews, L. C.; Williams, G. J. B. *J. Am. Chem. Soc.* **1977**, *99*, 6918–6923.
47. Stolzenberg, A. M.; Schussel, L. J.; Summers, J. S.; Foxman, B. M.; Petersen, J. L. *Inorg. Chem.* **1992**, *31*, 1678–1686.
48. Strauss, S. H.; Silver, M. E.; Long, K. M.; Thompson, R. G.; Hudgens, R. A.; Spartalian, K.; Ibers, J. A. *J. Am. Chem. Soc.* **1985**, *107*, 4207–4215.
49. Gallucci, J. C.; Swepston, P. N.; Ibers, J. A. *Acta Crystallogr.* **1982**, *B38*, 2134–2139.
50. Scheidt, W. R.; Lee, Y. J. *Structure and Bonding*; Buchler, J. W., Ed.; Springer: Berlin, 1987; Vol. 64, pp 1–70.
51. Jentzen, W.; Turowska-Tyrk, I.; Scheidt, W. R.; Shelnutt, J. A. *Inorg. Chem.* **1996**, *35*, 3559–3567.
52. Bruker-Nonius. *SAINT+ version 7.07B*; Bruker-Nonius: Madison, WI, 2004.
53. Bruker-Nonius. *SADABS version 2.10*; Bruker-Nonius: Madison, WI, 2004.
54. Altomare, A.; Cascarano, G.; Giacovazzo, C.; Guagliardi, A.; Burla, M. C.; Polidori, G.; Camalli, M. *J. Appl. Crystallogr.* **1994**, *27*, 435.
55. Bruker-AXS. *XL, SHELXTL version 6.12, UNIX*; Bruker-Nonius: Madison, WI, 2001.
56. Gabe, E. J.; Le Page, Y.; Charland, J.-P.; Lee, F. L.; White, P. S. *J. Appl. Crystallogr.* **1989**, *22*, 384–387.